Nonlinear tunneling in two-dimensional lattices

V. A. Brazhnyi[1], V. V. Konotop[1,2], V. Kuzmiak[3], and V. S. Shchesnovich[4]
[1] *Centro de Física Teórica e Computacional, Universidade de Lisboa, Complexo Interdisciplinar, Avenida Professor Gama Pinto 2, Lisboa 1649-003, Portugal*
[2] *Departamento de Física, Faculdade de Ciências, Universidade de Lisboa, Campo Grande, Ed. C8, Piso 6, Lisboa 1749-016, Portugal.*
[3] *Institute of Photonics and Electronics, v.v.i., Czech Academy of Sciences, Chaberska 57, 182 51 Prague 8, Czech Republic*
[4] *Instituto de Física - Universidade Federal de Alagoas, Maceió AL 57072-970, Brazil*

We present thorough analysis of the nonlinear tunneling of Bose-Einstein condensates in static and accelerating two-dimensional lattices within the framework of the mean-field approximation. We deal with nonseparable lattices considering different initial atomic distributions in the highly symmetric states. For analytical description of the condensate before instabilities are developed, we derive several few-mode models, analyzing both essentially nonlinear and quasi-linear regimes of tunneling. By direct numerical simulations, we show that two-mode models provide accurate description of the tunneling when either initially two states are populated or tunneling occurs between two stable states. Otherwise a two-mode model may give only useful qualitative hints for understanding tunneling but does not reproduce many features of the phenomenon. This reflects crucial role of the instabilities developed due to two-body interactions resulting in non-negligible population of the higher bands. This effect becomes even more pronounced in the case of accelerating lattices. In the latter case we show that the direction of the acceleration is a relevant physical parameter which affects the tunneling by changing the atomic rates at different symmetric states and by changing the numbers of bands involved in the atomic transfer.

PACS numbers:

I. INTRODUCTION

Tunneling in weakly nonlinear systems with periodically varying coefficients is intrinsically related to instabilities and, therefore, from the physical point of view the phenomenon differs fundamentally from its linear counterpart. This has been suggested in Ref. [1], where the two-level model for the Landau-Zener (LZ) tunneling was introduced, and supported by the direct numerical simulations of the two-dimensional (2D) Gross-Pitaevskii (GP) equation [2] where resonant tunneling between bands was stimulated by the nonlinearity rather than by the linear force and therefore termed as a *nonlinear* tunneling. LZ tunneling has also been extensively studied in a number of experiments carried out with Bose-Einstein condensates (BECs) loaded in moving optical lattices (OLs) [3, 4], where in particular, it was found that one can distinguish two situations corresponding to the instability regime and to the regime of Bloch oscillations. In Ref. [5] destructive effect of the nonlinearity in Wannier-Stark problem was investigated numerically. Very recently several experimental results were reported where resonant tunneling in tilted lattice was observed [6] and the role of asymmetry of the OL on the tunneling was studied [7].

The problem of tunneling has been addressed theoretically in two different limiting cases. In the case of a shallow lattice the tunneling was considered within the framework of the phenomenological models suggested in [8] and later on thoroughly analyzed and improved in [9]. The model accounting spatial dependence of the realistic field, but still based on the two-level approach was developed in [1]. While analytical description of the crossover among the above limiting cases is hardly achievable, to the best of authors knowledge there exist no direct numerical simulations allowing one to verify validity of each of the models and/or to study the transient regimes, and no generalization of the above theories on 2D and 3D lattices exists as yet, in contrast to the case of the linear tunneling that is well studied in multidimensional settings [10, 11]. Such a generalization is the main goal of the present paper.

The work is organized as follows. In Sec. II we outline the statement of the problem, presenting the analytical models with different types of the lattices. In Sec. III we deal with various cases of LZ, inter-band, and intra-band tunneling of matter waves in a deep OL, reducing the GP equation to different two– and three–level models. LZ tunneling in a shallow lattice is considered in Sec. IV. Numerical simulations of different types of tunneling in 2D lattices are described in Sec. V. The results obtained are summarized in Conclusion.

II. STATEMENT OF THE PROBLEM

We start with the dimensionless 2D GP equation

$$i\partial_t\psi = -\Delta\psi + V(\mathbf{r},t)\psi + \sigma|\psi|^2\psi, \qquad (1)$$

where time t and coordinates $\mathbf{r} = (x, y)$ are measured in units $2/\omega_z$ and $\ell_z = \sqrt{\hbar/m\omega_z}$, respectively, with ω_z being the linear harmonic oscillator frequency. $\sigma = \mathrm{sign}\, a_s$ where a_s is the scattering length of the condensate. The dimensionless wave function $\psi(\mathbf{r})$ is normalized as follows

$N = \int |\psi|^2 d^2\mathbf{r}$, where $N = 4\sqrt{2\pi}a_s N_{at}/\ell_z$ and N_{at} is a real number of atoms. The OL potential reads

$$V(\mathbf{r},t) = 2V_0[\cos^2(x - a_x t^2) + \cos^2(y - a_y t^2) + 2\varepsilon \cos(x - a_x t^2)\cos(y - a_y t^2)], \quad (2)$$

where the amplitude V_0 is measured in terms of recoil energy and $\varepsilon = \mathbf{e}_1 \cdot \mathbf{e}_2$. OL is assumed to be created by the two pairs of the counter-propagating beams with the polarization vectors $\mathbf{e}_{1,2}$, which are accelerating in the directions orthogonal to the polarization, where $\mathbf{a} = (a_x, a_y)$ denotes the acceleration (for description of experimental realization of multidimensional lattices see e.g. [12]).

For the next consideration it is convenient to make a substitution

$$\Psi = e^{i(2V_0 t + (\mathbf{r} - \mathbf{a}t^2)\mathbf{a}t + a^2 t^2/3)}\psi, \quad (3)$$

to introduce new independent variables $\tilde{\mathbf{R}} = \mathbf{r} - \mathbf{a}t^2$ and $T = t$, and to rewrite Eq. (1) in the form

$$i\partial_T \Psi = -\Delta_{\tilde{\mathbf{R}}}\Psi + (\mathbf{a} \cdot \tilde{\mathbf{R}})\Psi + V(\tilde{\mathbf{R}})\Psi + \sigma|\Psi|^2\Psi, \quad (4)$$

where the potential is time-independent:

$$V(\tilde{\mathbf{R}}) = V_0 \left[\cos(2\tilde{X}) + \cos(2\tilde{Y}) + 4\varepsilon \cos(\tilde{X})\cos(\tilde{Y})\right]. \quad (5)$$

It turns out, however that the laboratory system of coordinates, where $\tilde{\mathbf{R}}$ is the radius-vector, is not the most convenient frame for development of the theory. This stems from the fact that a nonseparable lattice possesses an elementary cell with boundaries that are rotated with respect to the axes of the laboratory system. This is illustrated in Fig. 1 where we show the OL given by (5). The simple square lattice has the period $\sqrt{2}\pi$ which is rotated by the angle $\pi/4$ with respect to the laboratory system. In Fig. 1 (a) besides the primitive translation vectors $\mathbf{l}_1 = \sqrt{2}\pi(1,1)$ and $\mathbf{l}_2 = \sqrt{2}\pi(-1,1)$, we depict in the inset the basis vectors $\mathbf{b}_1 = 1/\sqrt{2}(1,1)$ and $\mathbf{b_2} = 1/\sqrt{2}(-1,1)$ of the reciprocal lattice which define the first Brillouin zone (BZ).

Therefore it is convenient to introduce the rotated coordinate system [11] defining $X = \tilde{X} + \tilde{Y}$ and $Y = \tilde{X} - \tilde{Y}$. In the new coordinates the potential (5) reads as

$$V(\mathbf{R}) = 2\varepsilon V_0 \left(\cos X + \cos Y + \varepsilon^{-1}\cos X \cos Y\right) \quad (6)$$

and represents a simple square lattice with the primitive translation vectors parallel to the rotated X and Y axes. In the new frame the GP equation reads as

$$i\partial_T \Psi = -2\Delta_{\mathbf{R}}\Psi + (\mathbf{a}' \cdot \mathbf{R})\Psi + V(\mathbf{R})\Psi + \sigma|\Psi|^2\Psi. \quad (7)$$

where $\mathbf{a}' = ((a_x + a_y)/2, (a_x - a_y)/2)$.

In the linear case inter-band tunneling represents a possibility for a particle to pass from one energetic band to another. In 1D lattice this may occur due to the linear potential (the LZ tunneling), which can be interpreted in terms of changing the slope of the gap edges, leading to

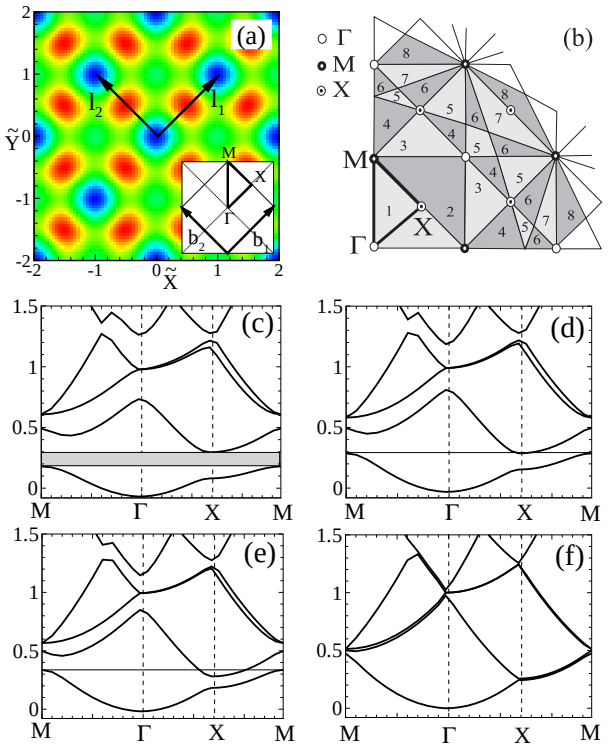

FIG. 1: (Color online) (a) Contour plot of the potential given by Eq. (5) with $V_0 = -0.55$ and $\varepsilon = 0.25$. In the inset we display the primitive vectors $\mathbf{b}_{1,2}$ of the reciprocal lattice, as well as the first BZ with the high symmetry points Γ, X, and M. (b) The eight lowest BZs with positions of high-symmetry points (only the first quadrant is shown). (c-f) Structures of the $E(q)$ for different amplitudes such as in (c) $V_0 = -0.55$ (full gap), in (d) $V_0 = -0.3823$ (vanishing gap), in (e) $V_0 = -0.3$ (overlapping of the first and second bands), in (f) $V_0 = -0.05$ (shallow lattice).

equal "effective" energies of the initial and the final steps (see e.g. [13]). In 2D and 3D lattices a particle can tunnel even without applying a linear force: in particular, in the case of a closed gap when initial and final states satisfy the energy and quasi-momentum conservation laws:

$$E_1 = E_2 \quad \text{and} \quad \mathbf{q}_1 - \mathbf{q}_2 = \mathbf{Q}, \quad (8)$$

hereafter $\mathbf{Q}$ is an arbitrary vector of the reciprocal lattice.

Even weak nonlinearity changes the situation dramatically. First, it can couple in a resonant way two (or more) states, which do not satisfy the energy and momentum conservation laws (8). This occurs due to process of *four-wave mixing*, which is efficient between the modes possessing the same group velocity. Second, the nonlinearity results in distinct stability properties of the different states, which in particular lead to asymmetric tunneling, i.e. to dependence of the tunneling on the initial conditions [1, 2]. We therefore use the term the *nonlinear tunneling* in order to highlight essentially new features of the phenomenon.

In this context we recall that accounting spatial depen-

dence of the models describing tunneling becomes highly relevant even in one-dimensional case where instabilities and nonexponential decay rate take place (see Refs. [1] and [5, 14], respectively).

III. FINITE-MODE APPROXIMATION. DEEP LATTICES.

A. Basic notations.

The theory developed in the present section is restricted neither by the cos-like potential as that of considered in (4) nor by the 2D case. We, however, limit ourselves only to the 2D case (3D generalization is straightforward but more cumbersome) and, therefore, by choosing the geometry of the square lattice, we first consider Eq. (7) with a more general periodic potential $V(\mathbf{R})$: $V(\mathbf{R}) = V(\mathbf{R} + \mathbf{l}_j)$, where $\mathbf{l}_j$ $(j = 1, 2)$ are the orthonormal lattice vectors. For the analysis of particular cases, we, however, always refer to the specific equation (4), (5).

We hereafter consider the lattice to be large enough in each direction, what allows us to follow the standard practice to consider effects independent on boundary conditions by choosing the most convenient ones, specifically we impose the cyclic boundary conditions.

In the analytical part of the present paper we deal only with the rotated system $\mathbf{R}$ considering $\Delta_{\mathbf{R}} \equiv \nabla^2$ where $\nabla \equiv (\partial_X, \partial_Y)$. We also use the derivative with respect to other variables indicating them by subindices, e.g. $\nabla_{\mathbf{q}} = (\partial_{q_X}, \partial_{q_Y})$.

In the weakly nonlinear case the associated linear spectral problem

$$\mathcal{L}\varphi_{\alpha\mathbf{q}}(\mathbf{R}) = E_\alpha(\mathbf{q})\varphi_{\alpha\mathbf{q}}(\mathbf{R}), \qquad \mathcal{L} \equiv -2\nabla^2 + V(\mathbf{R}) \quad (9)$$

plays a prominent role. Here $\mathbf{q}$ is the wavevector in the reduced BZ: $q_{X,Y} \in [-q_B, q_B]$ with $q_B = 1/2$, $\alpha = 1, 2, ...$ is a band number, $\varphi_{\alpha\mathbf{q}}(\mathbf{R}) = e^{i\mathbf{q}\mathbf{R}}u_{\alpha\mathbf{q}}(\mathbf{R})$, where $u_{\alpha\mathbf{q}}(\mathbf{R})$ are periodic functions $u_{\alpha\mathbf{q}}(\mathbf{R}) = u_{\alpha\mathbf{q}}(\mathbf{R} + \mathbf{l}_j)$, are the Bloch functions (BFs).

We use the internal product defined by

$$\langle u \mid \hat{A} \mid v\rangle = \frac{1}{\mathcal{V}}\int_{\mathcal{V}} \bar{u}(\mathbf{r})\hat{A}v(\mathbf{r})d\mathbf{r}, \quad (10)$$

where $\hat{A}$ is an operator and $\mathcal{V}$ is the volume of the lattice. With the linear eigenvalue problem (9) we associate physically important quantities: the group velocity of a mode

$$\mathbf{v}_{\alpha\mathbf{q}} = \langle\varphi_{\alpha\mathbf{q}} \mid -4i\nabla \mid \varphi_{\alpha\mathbf{q}}\rangle = \nabla_{\mathbf{q}}E_\alpha(\mathbf{q}) \quad (11)$$

and the tensor of the inverse effective mass $\mathbf{M}^{-1}_{\alpha\mathbf{q}}$ with the entrees

$$(\mathbf{M}^{-1}_{\alpha\mathbf{q}})_{ij} = 4 - 8\sum_{\alpha_1\neq\alpha}\frac{\langle\varphi_{\alpha\mathbf{q}} \mid \partial_k \mid \varphi_{\alpha_1\mathbf{q}}\rangle\langle\varphi_{\alpha_1\mathbf{q}} \mid \partial_l \mid \varphi_{\alpha\mathbf{q}}\rangle}{E - E_{\alpha_1}(\mathbf{q})} = \frac{\partial^2 E_\alpha(\mathbf{q})}{\partial q_i \partial q_j}, \quad (12)$$

where $k, l = X, Y$ (see e.g. [15] for more details).

In the case where the lattice potential is not small, i.e. $V_0 \gtrsim 1$, we seek the solution of Eq. (7) in the form

$$\Psi = \sum_{j=1}\epsilon^j\psi_j, \quad (13)$$

where $\epsilon \ll 1$ is a small parameter and ψ_j are the functions of a scaled spatial, $\mathbf{r}_j = (x_j, y_j) = (\epsilon^j X, \epsilon^j Y)$, and temporal, $t_j = \epsilon^j T$, variables (here $j = 0, 1, ...$). By analogy we define $\nabla_j = \left(\partial_{x_j}, \partial_{y_j}\right)$. This approach is referred to as a multiple-scale expansion, which in the context of 2D BEC loaded in an OL was described in [15]. Below we explore some generalization of the expansion, including the linear force as well as resonant wave interactions in the consideration.

By substituting expansion (13) into Eq. (7), passing to the scaled independent variables, and gathering the terms of the same order of ϵ, up to ϵ^3 one obtains $(j = 1, 2, 3)$

$$\left(i\partial_{t_0} - \mathcal{L}\right)\psi_j = \mathcal{F}_j, \quad (14)$$

where $\mathcal{F}_1 = 0$, $\mathcal{F}_2 = -(i\partial_{t_1} + 4\nabla_0\nabla_1)\psi_1$, and

$$\mathcal{F}_3 = -(i\partial_{t_1} + 4\nabla_0\nabla_1)\psi_2 - (i\partial_{t_2} + 4\nabla_0\nabla_2 + 2\nabla_1^2)\psi_1 + \sigma|\psi_1|^2\psi_1.$$

Tunneling of atoms between two states, belonging to the bands α_1 and α_2 requires equality of the group velocities of the interacting modes (see e.g. [16]):

$$\mathbf{v}_1 = \mathbf{v}_2 = \mathbf{v} \quad (15)$$

what will be assumed in what follows.

Finally, to shorten notations, the BFs corresponding to the states coupled by tunneling will be denoted as $(j = 1, 2, 3)$ $\varphi_{\alpha_j\mathbf{q}_j} = \varphi_j$ (respectively $u_{\alpha_j\mathbf{q}_j} = u_j$).

B. Band structures

Focusing on the lowest bands, in Fig. 1 we show four qualitatively different configurations, which can be realized by varying the amplitude of the potential. They correspond to the existence of the full gap between the first and second lowest bands, indicated by shaded area in the panel (c); closed (or infinitesimally small) gap, indicated by the thin horizontal line in the panel (d); absence of a full gap in a relatively deep lattice shown in the panel (e); and the band structure associated with a shallow lattice depicted in the panel (f).

Different aspects of instabilities and inter-band transitions corresponding to the cases (c) of a full gap and (e) of absence of a gap, when resonance conditions of the four wave mixing are not satisfied, have been considered in [15] and [2], respectively, and they will not be addressed here. We only note that before instabilities are developed the problem is well described within the framework of the two-level model.

C. Nonlinear inter– and intra–band tunneling.

Let us start with the case of the *resonant* nonlinear tunneling between two different states having the same energy, i.e. satisfying the conditions

$$E_1 = E_2 = E \quad \text{and} \quad \mathbf{q}_1 = \mathbf{q}_2 + \mathbf{q}_2 - \mathbf{q}_1 + \mathbf{Q}. \quad (16)$$

Both (16) and (15) can always be achieved in all orthogonal lattices if one considers two X points related by the rotation by $\pi/2$: then $\mathbf{q}_1 = (q_B, 0)$ and $\mathbf{q}_2 = (0, q_B)$; and in lattices with a closed gap as it is shown in Fig. 1 (d): then $\mathbf{q}_1 = (q_B, 0)$ and $\mathbf{q}_2 = (q_B, q_B)$ and the points X and M are considered. The most significant difference between the mentioned two cases is that in the first case the effective masses of the both states have the same sign (and thus the respective Bloch states posses the same stability), while in the second case the effective masses have different signs (and one of the Bloch states is necessarily stable, while the other one is unstable).

We look for a solution of (14) with $j = 1$ in the form

$$\psi_1 = \left[A_1(\mathbf{r}_1, t_1)\varphi_1(\mathbf{r}_0) + A_2(\mathbf{r}_1, t_1)\varphi_2(\mathbf{r}_0)\right] e^{-iEt_0}, \quad (17)$$

where $A_j(x_1, t_1)$ are slowly varying amplitudes which depend on slow variables with the fastest ones being indicated explicitly. For the next step one expands (see Appendix A 2)

$$\psi_2 = \left[\sum_{\alpha\neq\alpha_1} B^{(1)}_\alpha(\mathbf{r}_1, t_1)\varphi_{\alpha\mathbf{q}_1}(\mathbf{r}_0) + \sum_{\alpha\neq\alpha_2} B^{(2)}_\alpha(\mathbf{r}_1, t_1)\varphi_{\alpha\mathbf{q}_2}(\mathbf{r}_0)\right] e^{-iEt_0}, \quad (18)$$

where $B_{\alpha\mathbf{q}}(\mathbf{r}_1, t_1)$ are slowly varying functions (we use a convention that all sums with respect to α are computed between $\alpha = 1$ and $\alpha = \infty$, with possible exclusions which are explicitly indicated. Substituting (18) in (14) with $j = 2$ and projecting on the states $\varphi_{1,2}$ we obtain

$$A_1 = A_1(\mathbf{r}_1 - \mathbf{v}t_1, t_2) \text{ and } A_2 = A_2(\mathbf{r}_1 - \mathbf{v}t_1, t_2)\,. \quad (19)$$

Projection on the rest of the states $\varphi_{\alpha\mathbf{q}}$ yields the expression for B (see Appendix A 2).

Passing to the third order we impose the orthogonality of $\mathcal{F}_3$ and ψ_1 and taking into account that the conditions (15) and (16) can be satisfied simultaneously only for high-symmetric points, e.g. the points Γ, X, and M, where the group velocity is zero, $\mathbf{v} = 0$ and the tensor of the inverse effective mass is diagonal, $\hat{\mathbf{M}}^{-1}_\alpha$ =diag$(M^{-1}_{\alpha,x}, M^{-1}_{\alpha,y})$. Then we obtain set of the equations

$$i\frac{\partial A_1}{\partial t_2} + \frac{1}{2}\nabla_1\hat{\mathbf{M}}^{-1}_1\nabla_1 A_1 - \tilde{\chi}_{12}\bar{A}_1 A_2^2 - \left(\chi_{11}|A_1|^2 + 2\chi_{12}|A_2|^2\right)A_1 = 0, \quad (20a)$$

$$i\frac{\partial A_2}{\partial t_2} + \frac{1}{2}\nabla_1\hat{\mathbf{M}}^{-1}_2\nabla_1 A_2 - \tilde{\chi}_{21}\bar{A}_2 A_1^2 - \left(\chi_{22}|A_2|^2 + 2\chi_{12}|A_1|^2\right)A_2 = 0, \quad (20b)$$

where we define the operator

$$\nabla_1\hat{\mathbf{M}}^{-1}_\alpha\nabla_1 \equiv \frac{1}{M_{\alpha,x}}\frac{\partial^2}{\partial x_1^2} + \frac{1}{M_{\alpha,y}}\frac{\partial^2}{\partial y_1^2}.$$

The nonlinearity coefficients are given by $(\alpha, \beta = 1, 2)$

$$\chi_{\alpha\beta} = \chi_{\beta\alpha} = \sigma\langle\varphi_\alpha\varphi_\beta \mid \varphi_\alpha\varphi_\beta\rangle, \quad (21)$$

$$\tilde{\chi}_{\alpha\beta} = \overline{\tilde{\chi}}_{\beta\alpha} = \sigma\langle\varphi_\alpha^2 \mid \varphi_\beta^2\rangle. \quad (22)$$

D. Nonlinear Landau-Zener tunneling.

The LZ tunneling is induced by the linear potential when there exists a full gap between bands. Being originated by the linear term it requires conservation of the linear momentum. In order to observe how the nonlinearity affects LZ tunneling, the linear force has to induce an effect of the same order as the nonlinearity. Since our approach is valid only for weak nonlinearity, both the linear force and the gap, through which tunneling is considered, have to be sufficiently small, as well. Thus we require

$$E_2 - E_1 = \epsilon^2\mathcal{E}\,, \quad \mathbf{q}_1 - \mathbf{q}_2 = \mathbf{Q}, \quad (23)$$

where $\mathcal{E} \lesssim 1$. Further, we assume that $\mathbf{a}' = \epsilon^2\widetilde{\mathbf{a}}$ with $|\widetilde{\mathbf{a}}| \sim 1$. Therefore, the linear force will appear only in the third order of the multiple-scale expansion.

The condition (23) together with the constraint (15) means that in a general situation LZ tunneling can occur either between the two symmetric points M, with $\mathbf{q}_1 = (q_B, q_B)$ and $\mathbf{q}_2 = (\pm q_B, \pm q_B)$, or between the points X, with $\mathbf{q}_1 = (q_B, 0)$ and $\mathbf{q}_2 = (0, \pm q_B)$, belonging to different boundaries of a gap. Therefore, as before the group velocity is zero, i.e. $\mathbf{v} = 0$.

Taking into account that now the energies of the two states are different, we perform the multiple-scale expansion for the superposition of the states

$$\psi_1 = A_1(\mathbf{r}_1, t_1)\varphi_1(\mathbf{r}_0)e^{-iE_1t_0} + A_2(\mathbf{r}_1, t_1)\varphi_2(\mathbf{r}_0)e^{-iE_2t_0} \quad (24)$$

and repeat the steps of derivation of (20) (see Appendix A1). Specifically, the second order term now has the form (here $\mathbf{q} = \mathbf{q}_1$)

$$\psi_2 = \sum_\alpha \left[B^{(1)}_{\alpha\mathbf{q}}(\mathbf{r}_1, t_1)\varphi_{\alpha\mathbf{q}}e^{-iE_1t_0} + B^{(2)}_{\alpha\mathbf{q}}(\mathbf{r}_1, t_1)\varphi_{\alpha\mathbf{q}}e^{-iE_2t_0}\right]. \quad (25)$$

The requirement of the absence of the secular terms results in

$$i\frac{\partial A_1}{\partial t_2} + \frac{1}{2}\nabla_1\hat{\mathbf{M}}^{-1}_1\nabla_1 A_1 - \kappa e^{i\mathcal{E}t_2}A_2 - \left(\chi_{11}|A_1|^2 + 2\chi_{12}|A_2|^2\right)A_1 = 0, \quad (26a)$$

$$i\frac{\partial A_2}{\partial t_2} + \frac{1}{2}\nabla_1\hat{\mathbf{M}}^{-1}_2\nabla_1 A_2 - \kappa e^{-i\mathcal{E}t_2}A_1 - \left(\chi_{22}|A_2|^2 + 2\chi_{12}|A_1|^2\right)A_2 = 0, \quad (26b)$$

where the coupling coefficient κ is given by

$$\kappa = \widetilde{\mathbf{a}}\langle\varphi_1|\mathbf{r}|\varphi_2\rangle = \widetilde{\mathbf{a}}\langle\varphi_2|\mathbf{r}|\varphi_1\rangle\,. \tag{27}$$

In the case, when the Rabi frequency defined by κ significantly exceeds the rotational frequency $\mathcal{E}$, i.e. when $\mathcal{E} \ll \kappa$, the time dependence of the coupling term can be neglected.

E. Interplay between Landau-Zener tunneling and nonlinear tunneling.

In the cases considered above we singled out one resonant process, which is dominant for the atomic migration between the bands. Meantime, one can create a situation where there exist two competing processes. This, in particular, may happen in the structure, depicted in Fig.1 (d), when a linear force is applied allowing for resonant nonlinear LZ tunneling. In this particular case, the state M of the lowest band (state "1" below) through the linear force is coupled to the state M of the second band (state "2" below) and through the four-wave mixing process with the state X of the second band (state "3" below). The matching conditions now read

$$E_1 = E_3 = E_2 - \epsilon^2\mathcal{E}, \tag{28a}$$
$$\mathbf{q}_1 = \mathbf{q}_2 + \mathbf{Q}, \quad \mathbf{q}_1 = \mathbf{q}_3 - \mathbf{q}_3 + \mathbf{q}_1 + \mathbf{Q}. \tag{28b}$$

To take into account all resonant processes in this case a three-mode model is required. Therefore, we seek a solution of Eq. (14) in the form

$$\psi_1 = [A_1(\mathbf{r}_1,t_1)\varphi_1(\mathbf{r}_0) + A_3(\mathbf{r}_1,t_1)\varphi_3(\mathbf{r}_0)]e^{-iE_1t_0} + A_2(\mathbf{r}_1,t_1)\varphi_2(\mathbf{r}_0)e^{-iE_2t_0}. \tag{29}$$

The algebra similar to one described above, results in the following set of equations for slowly varying amplitudes

$$i\frac{\partial A_1}{\partial t_2} + \frac{1}{2}\nabla_1\hat{\mathbf{M}}_1^{-1}\nabla_1 A_1 - \kappa e^{i\mathcal{E}t_2}A_2 - \left(\chi_{11}|A_1|^2 + 2\chi_{12}|A_2|^2 + 2\chi_{13}|A_3|^2\right)A_1 - \tilde{\chi}_{13}\bar{A}_1A_3^2 = 0, \tag{30a}$$
$$i\frac{\partial A_2}{\partial t_2} + \frac{1}{2}\nabla_1\hat{\mathbf{M}}_2^{-1}\nabla_1 A_2 - \kappa e^{-i\mathcal{E}t_2}A_1 - \left(\chi_{22}|A_2|^2 + 2\chi_{12}|A_1|^2 + 2\chi_{13}|A_3|^2\right)A_2 = 0, \tag{30b}$$
$$i\frac{\partial A_3}{\partial t_2} + \frac{1}{2}\nabla_1\hat{\mathbf{M}}_3^{-1}\nabla_1 A_3 - \left(\chi_{22}|A_2|^2 + 2\chi_{12}|A_1|^2 + 2\chi_{13}|A_3|^2\right)A_3 - \tilde{\chi}_{31}\bar{A}_3A_1^2 = 0. \tag{30c}$$

We mention that resonant coupling of three states (the two X states and one M state) is also possible in the case depicted Fig.1 (d). Detailed study of the coupled-mode equations for the slow envelopes can be found in [17].

IV. FINITE-MODE APPROXIMATION. SHALLOW LATTICE.

The LZ tunneling in a shallow accelerated lattice, $V_0 \ll 1$, can be most conveniently considered in the rotated coordinate system, i.e. Eq. (7) with the potential defined by Eq. (6). For the sake of convenience, we normalize the wave function as $\Psi = \psi/N^{1/2}$, and introduce the nonlinearity coefficient $g = \sigma N$, with the assumption that $|g| \ll 1$. Now the BFs can be approximated by linear combinations of the plane waves (see e.g. [9]), thus one can use the plane waves as the basis of expansion.

We assume that the order parameter of a BEC has the Fourier spectrum consisting of narrow peaks, whose width being much smaller than the size of the BZ. In this case, similar to Houston's approach in the theory of accelerating electrons [18], the order parameter is taken in the form

$$\Psi(\mathbf{R},t) = e^{i\mathbf{q}(t)\mathbf{R}}\sum_j C_j(t)e^{i\mathbf{Q}_j\mathbf{R}}, \tag{31}$$

where the sum consists of the plane waves satisfying the resonant conditions (8), $\mathbf{Q}_j$ are the reciprocal lattice vectors.

Linear LZ tunneling is a result of Bragg resonance and occurs when the Bloch index $\mathbf{q}(t)$ crosses one of the Bragg planes (a Bragg plane in 2D is a line passing through the mid-point of a reciprocal lattice vector $\mathbf{Q}_j$, taken from the Γ-point, and perpendicular to it). The lattice defined by the potential (6) admits two-fold (i.e. quasi 1D) and four-fold Bragg resonances (for more details see Ref. [10]).

A weak nonlinearity can be accounted in the following way [9]: the lattice potential and the nonlinear term are considered as an effective time-dependent lattice potential $V_{\text{eff}} \equiv V(\mathbf{R}) + g|\Psi(\mathbf{R},t)|^2$, where the order parameter is assumed periodic in $\mathbf{R}$. Thus, in this approach, nonlinearity does not change the relation between LZ tunneling and Bragg resonances.

The potential can be rewritten in terms of the recip-

rocal lattice vectors as

$$V = \varepsilon V_0[e^{i\mathbf{Q}_{1,0}\mathbf{R}} + e^{i\mathbf{Q}_{0,1}\mathbf{R}}] + \frac{V_0}{2}[e^{i\mathbf{Q}_{1,1}\mathbf{R}} + e^{i\mathbf{Q}_{1,-1}\mathbf{R}}] + c.c.. \tag{32}$$

Here $\mathbf{Q}_{1,0} = (2q_B, 0)$, $\mathbf{Q}_{0,1} = (0, 2q_B)$, and $\mathbf{Q}_{1,\pm 1} = \mathbf{Q}_{1,0} \pm \mathbf{Q}_{0,1}$ (recall that $q_B = 1/2$). The Bragg planes can thus be indexed accordingly, for instance, the Bragg plane $B_{1,0}$ corresponds to $\mathbf{Q}_{1,0}$.

Two-fold Bragg resonances. The two-fold Bragg resonance occurs at any one of the Bragg planes away from the $\mathcal{O}(V)$-neighborhood of the high-symmetry points, (i.e. the points of intersection of two or more Bragg planes), for instance the M-points. By keeping only the resonant terms we obtain:

$$\Psi = C_1(t)e^{i\mathbf{q}(t)\mathbf{R}} + C_2(t)e^{i(\mathbf{q}(t)-\mathbf{Q})\mathbf{R}}, \tag{33}$$

$$\begin{aligned} V_{\text{eff}} = \quad & (\hat{V}_{\mathbf{Q}} + gC_1\bar{C}_2)e^{i\mathbf{Q}\mathbf{R}} + (\hat{V}_{-\mathbf{Q}} + g\bar{C}_1C_2)e^{-i\mathbf{Q}\mathbf{R}} \\ & + g(|C_1|^2 + |C_2|^2), \end{aligned} \tag{34}$$

where $\hat{V}_{\mathbf{Q}}$ is the Fourier amplitude corresponding to $\mathbf{Q}$. Substituting the expressions (33) and (34) into equation (7) we get $\dot{\mathbf{q}} = -\mathbf{a}'$, which cancels the linear potential, and the set of the equations for the amplitudes C_1 and C_2. The latter can be simplified when we use the conservation of the norm, in this case $|C_1|^2 + |C_2|^2 = 1$, and the phase transformation $C_j = e^{-i\phi}c_j$ with $\dot{\phi} = 3g/2 + 2(\mathbf{q}_{\text{res}}^2 + (\mathbf{a}')^2t^2)$, where we denote $\mathbf{q}_{\text{res}}$ the crossing point of the corresponding Bragg plane. Setting $\mathbf{q}(t) = \mathbf{q}_{\text{res}} - \mathbf{a}'t$ (i.e. the resonance is set at $t = 0$), we obtain the set of the equations ($j = 1, 2$)

$$i\dot{c}_j = (-1)^j \left[4\mathbf{q}_{\text{res}}\mathbf{a}'t + \frac{g}{2}(|c_j|^2 - |c_{3-j}|^2)\right] c_j + \hat{V}_{\mathbf{Q}}c_{3-j}, \tag{35}$$

The system (35) is identical to that in the 1D lattice [8]. The only signature of the higher dimensionality in the system (35) is that of the dependence of the sweep amplitude (i.e. $4\mathbf{q}_{\text{res}}\mathbf{a}'$) on the angle between the Bloch index of the crossing point and the acceleration.

In the linear case, $g = 0$, the tunneling probability P corresponding to the system (35) is given by the well-known Landau-Zener-Majorana formula [19]:

$$P \equiv |c_1(\infty)|^2 = \exp\left\{-\frac{\pi|\hat{V}_{\mathbf{Q}}|^2}{4|\mathbf{q}_{\text{res}}\mathbf{a}'|}\right\}, \tag{36}$$

where it is assumed that "initially" $|c_1(-\infty)| = 1$. For instance, at the X-point we get $P_{\text{X}} = e^{-\pi\varepsilon^2V_0^2/(a_x+a_y)}$.

Four-fold Bragg resonances. This resonance occurs at the intersection of two Bragg planes, for instance at the M-point [the other case is at the Γ-point, see Fig.1 (f)]. Using the lattice potential in (32), the resonant part of the order parameter

$$\Psi_{\text{res}} = \sum_{j=1}^{4} C_j(t)e^{i(\mathbf{q}_j - \mathbf{a}'t)\mathbf{R}}, \tag{37}$$

where $\mathbf{q}_1 = \mathbf{Q}_{1,1}/2$, $\mathbf{q}_2 = \mathbf{Q}_{-1,-1}/2$, $\mathbf{q}_3 = \mathbf{Q}_{-1,1}/2$, and $\mathbf{q}_4 = \mathbf{Q}_{1,-1}/2$ connect the Γ and M points, and the relations $\mathbf{Q}_{1,1}\mathbf{a}' = a_x$ and $\mathbf{Q}_{1,-1}\mathbf{a}' = a_y$ we obtain a set of the equations for the Fourier amplitudes C_j of the order parameter. The system is simplified after the transformation $C_j = e^{-i\phi}c_j$ with $\dot{\phi} = g + 2[\mathbf{q}_1^2 + (\mathbf{a}')^2t^2]$ and using of the norm conservation $\sum_j |C_j|^2 = 1$:

$$i\dot{c}_1 = \left(-2a_xt - g|c_1|^2\right)c_1 + \frac{V_0}{2}c_2 + \varepsilon V_0(c_3 + c_4) + 2g\bar{c}_2c_3c_4, \tag{38}$$

$$i\dot{c}_2 = \left(2a_xt - g|c_2|^2\right)c_2 + \frac{V_0}{2}c_1 + \varepsilon V_0(c_3 + c_4) + 2g\bar{c}_1c_3c_4, \tag{39}$$

$$i\dot{c}_3 = \left(2a_yt - g|c_3|^2\right)c_3 + \frac{V_0}{2}c_4 + \varepsilon V_0(c_1 + c_2) + 2gc_1c_2\bar{c}_4, \tag{40}$$

$$i\dot{c}_4 = \left(-2a_yt - g|c_4|^2\right)c_4 + \frac{V_0}{2}c_3 + \varepsilon V_0(c_1 + c_2) + 2gc_1c_2\bar{c}_3. \tag{41}$$

In the linear case, $g = 0$, one can use the general formula for the tunneling probability [20], $P = |c_j(\infty)|^2 = \exp\left\{-2\pi\sum_{m\neq j}\frac{|\Delta_{mj}|^2}{|\nu_m - \nu_j|}\right\}$ for $|c_j(-\infty)| = 1$, where ν_j is the strongest sweep amplitude and Δ_{mj} is the cross-coupling term. For instance, in the case of $|a_x| > |a_y|$ we get for $P = |c_1(\infty)|^2$:

$$P = \exp\left\{-\frac{\pi V_0^2}{8|a_x|} - \frac{\pi\varepsilon^2V_0^2}{|a_x + a_y|} - \frac{\pi\varepsilon^2V_0^2}{|a_x - a_y|}\right\}, \tag{42}$$

with the initial condition $|c_1(-\infty)| = 1$. The same formula is true for $P = |c_4(\infty)|^2$ with $|c_4(-\infty)| = 1$. The physical meaning of Eq. (42) is clear: it determines the

fraction of BEC atoms which pass through the border of the first BZ at the M-point by continuously increasing their quasimomentum (BEC atoms leave the first BZ also through the side M-points, with the corresponding fractions given by the Fourier amplitudes c_3 and c_4).

In the special case of $a_x = a_y = a$ using formula (36), we obtain the probability of the transition in the form

$$P = \exp\left\{-\pi\frac{(1/2+\varepsilon)^2 V_0^2}{2|a|}\right\}. \qquad (43)$$

Finally, the squared amplitudes $|c_j(t)|^2$ of the LZ system can be compared with the powers of the Fourier peaks in the full PDE (defined as the integral of the modulus squared of Fourier amplitude) – see Fig. 11 of Section V C.

V. NUMERICAL RESULTS

The theory of tunneling developed in the preceding sections is based on the two– (few –) mode approximation. As it has been shown in [2] on an example of inter-band tunneling between two initially populated states, this approach is valid until instability is developed. In general, when initially only one of the states is populated or when one assumes several populated states, that are not connected by some of the resonant conditions, the theoretical model requires verification.

In this Section we address problems of tunneling starting with only one populated state in a stationary lattice and of LZ tunneling in an accelerating lattice with different directions of the lattice acceleration and different lattice depths. We impose the initial conditions in the form $\psi(x,0) = \sum_{\alpha,\mathbf{q}} \sqrt{r_{\alpha\mathbf{q}}}\,\varphi_{\alpha\mathbf{q}}$, where summation is taken up to the eight lowest bands, $\alpha = 1, ..., 8$, and over the symmetric points which we denote as $\mathbf{q}_\Gamma = (0,0)$, $\mathbf{q}_\mathrm{X} = (\pm 1/2, \pm 1/2)$, $\mathbf{q}_{\mathrm{X}'} = (\pm 1/2, \mp 1/2)$, and $\mathbf{q}_\mathrm{M} = [(0,\pm 1),(\pm 1,0)]$. We study evolution of the positive quantities $r_{\alpha\mathbf{q}}$ representing populations of the respective states. Also we use the notation Y_α for a point Y=(X, M, Γ) of α-th band.

In all numerical simulations we solve the original GP equation (1), i.e. our results are obtained directly for the accelerating lattice (2). We use the Crank-Nicolson scheme with periodic boundary conditions on the grid with 400×400 points and with 20 periods of the OL in each direction (such a size of the lattice lattice is sufficiently large to allow one to observe volume phenomena that are not affected by the specific type of the boundary conditions). Finally, we assume inter-atomic interactions to be repulsive, i.e. $\sigma = 1$.

For a typical experimental setup with 10^4 atoms having scattering length of order of 0.01 nm (achievable by means of Feshbach resonance) and with transversal size of the cloud $\ell_z \approx 0.3\,\mu$m our numerical unit of time corresponds approximately to 0.25 ms. Also, in what follows we use the normalization constants $N = 10$ and $N = 20$ [defined after (1)] what corresponds to 3×10^4 and 6×10^4 of real atoms.

A. Stationary optical lattice

1. *Non-tunneling regime and the modulational instability*

We start with examining the case where energy of the initially populated M_1-point is the same as that of X_2-point which is not populated at $t = 0$. This is the case described by (16). Now in contrast to the situation described in [2], now it is *a priori* not known which mode (or modes) the energy will be transferred to. Thus one may expect tunneling between bands, induced by modulational instability (MI) in the state M_1(since the effective masses $M_{1,x}$ and $M_{1,y}$ are negative and $\sigma = 1$). The results are shown in Fig. 2.

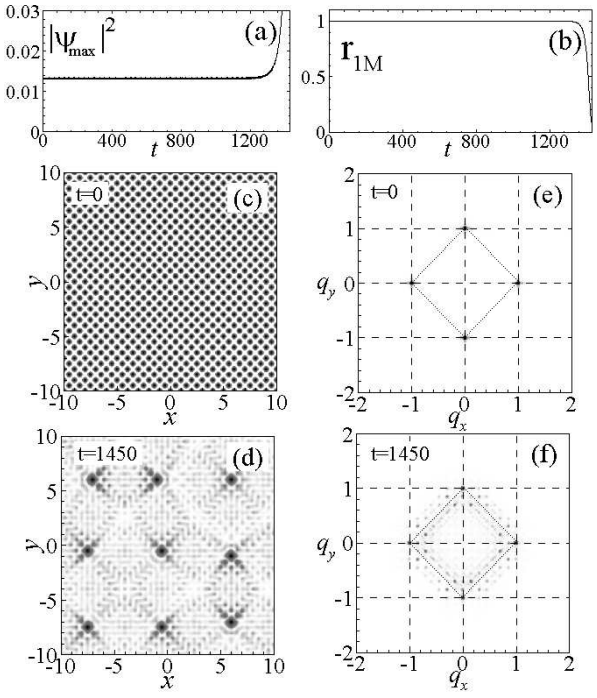

FIG. 2: (Color online) Development of MI starting in the M_1-point. In (a) temporal behavior of the density maximum [at $t \approx 1300$ (what corresponds 0.325 s, i.e. to experimentally feasible time) the MI starts to develop] and in (b) the dynamics of the population of the M_1-state is shown (populations of the higher bands in the Γ-, X- and M-points are smaller than 10^{-5}). The parameters are as follows: $V_0 = -0.3823$, $\varepsilon = 0.25$, $N = 10$. In (c), (d) density profiles and in (e), (f) their Fourier transformations at different times are shown.

The most relevant result stems from the fact that even after the MI is developed the populations of the symmetric states of the upper bands, including the states X_2 are negligibly small. It means, that in spite of the resonant conditions (16) being satisfied, tunneling does not occur, i.e. the expected scenario, which is described

above, is not realized. In order to investigate the dynamics in the Fourier space, we have computed the Fourier transform of the wave function at different moments of time see Fig. 2 (e), (f). In the process of the development of MI the atoms spread out along the boundary of the first BZ. Dispersion spreading proceeds until the MI is developed. Only the unstable state M_1 imprints its signature in the symmetry of the developed structure [see Fig. 2 (d)] and therefore its pattern closely resembles the structures emerged from the unstable states in a separable lattice (c.f. with Fig. 7 in the Ref.[15]).

2. *Bloch intra-band tunneling at the X_2-point*

We obtained perhaps even more surprising results when in the lattice with the band structure depicted in Fig. 1 (d) we initially populated a stable state X_2 that possesses two positive effective masses. In Figs. 3 and 4 one can observe exchange of particles between the two doubly degenerate X_2-points which are related by the rotation $\pi/2$ and referred to as X_2 and X_2' below. In other words the system develops intra-band tunneling instead of the inter-band one.

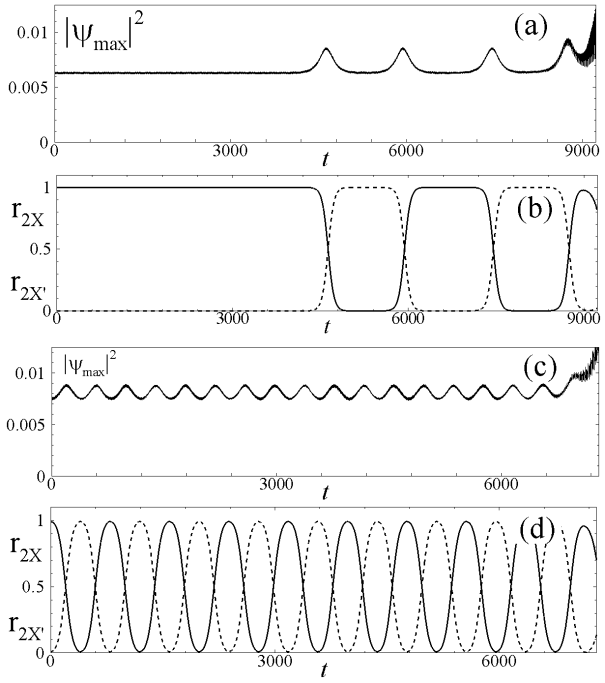

FIG. 3: Time dependence of the maximum of the density amplitude [(a),(c)] and populations r_{2X} (solid line) and $r_{2X'}$ (dashed line) [(b),(d)] of the X-states of the second band in the case when in (a), (b) initially all particles are in the X_2-state and in (c), (d) initially $r_{2X} = 0.99$ and $r_{2X'} = 0.01$. In (a) at $t \approx 9000$ (≈ 2.3 s) and in (c) at $t \approx 7300$ (≈ 1.8 s) the MI starts to develop. The ratio between the time intervals when the particles populate X- or X′-states in (b) is ≈ 1.2. The parameters are as follows: $\Lambda \approx 0.792$, $V_0 = -0.3823$, $\varepsilon = 0.25$, $N = 10$.

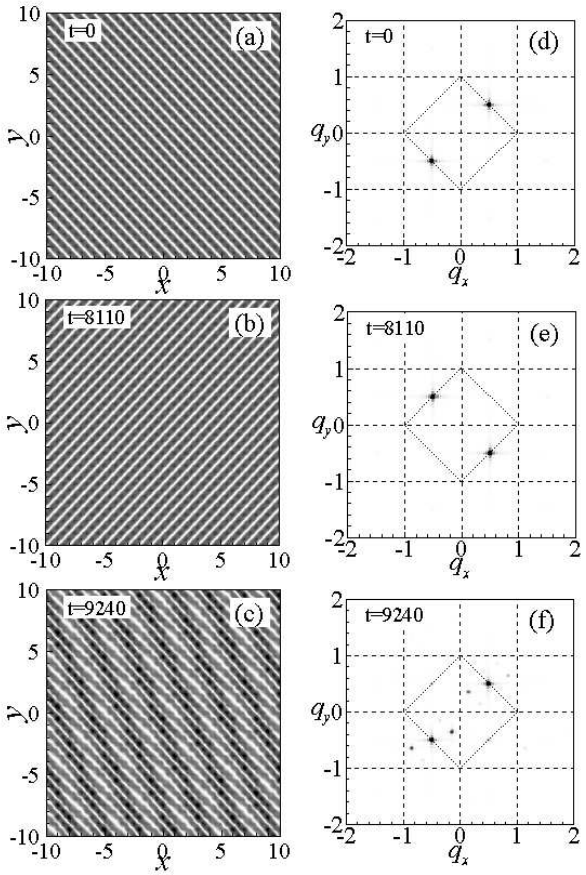

FIG. 4: (Color online) In (a)-(c) density profiles and in (d)-(f) their Fourier transformations at different times corresponding to Fig.3 (a), (b) are shown.

This picture agrees with the theory developed in Sec. III C. Indeed, first we recall that the both states X_2 are stable, while the state M_1 having the same energy is unstable. Next, we consider (20) and take into account that initially the envelopes $A_{1,2} \equiv A_{1,2}(t_2)$ are independent on spatial coordinates: $\nabla_1 A_{1,2} \equiv 0$. This allows us to reduce the system of PDEs to a Hamiltonian system with the Hamiltonian

$$H_{eff} = \frac{1}{2}\chi_{11}|A_1|^4 + \frac{1}{2}\chi_{11}|A_2|^4 + 2\chi_{12}|A_1|^2|A_2|^2 + \chi_{12}\bar{A}_1^2 A_2^2 + \chi_{12}\bar{A}_2^2 A_1^2 . \quad (44)$$

Here we have taken into account the symmetry of the lattice resulting in $\chi_{11} = \chi_{22}$ and $\chi_{12} = \tilde{\chi}_{12} = \chi_{21} = \tilde{\chi}_{21}$ [see Eqs. (21) and (22)].

Since the derived dynamics preserves the "total number of particles" $\mathcal{N} = \mathcal{N}_1 + \mathcal{N}_2$, where $\mathcal{N}_j = |A_j|^2$ we introduce the population imbalance $z = (|A_2|^2 - |A_1|^2)/\mathcal{N}$, the relative argument $\phi = 2\arg(A_1\bar{A}_2)$, the parameter $\Lambda = \chi_{21}/\chi_{11}$, as well as the renormalized time $\tau = \chi_{11}\mathcal{N}t_2$. Now the dynamical system can be rewritten

in the form

$$\frac{dz}{d\tau} = \Lambda(1-z^2)\sin\phi = \frac{\partial H_{eff}}{\partial \phi}, \quad (45)$$

$$\frac{d\phi}{d\tau} = 2z(1-\Lambda\cos\phi - 2\Lambda) = -\frac{\partial H_{eff}}{\partial z}, \quad (46)$$

where the effective Hamiltonian has the form

$$H_{eff} = (1-z^2)(1-\Lambda\cos\phi - 2\Lambda)\,. \quad (47)$$

For the next consideration one should keep in mind that the dependent variables are bounded: $-1 \le z \le 1$ and $0 \le \phi \le 2\pi$. From Cauchy inequality $\langle|\varphi_\alpha|^2|\varphi_\beta|^2\rangle \le \sqrt{\langle|\varphi_\alpha|^4\rangle\langle|\varphi_\beta|^4\rangle}$, it follows that $0 \le \Lambda \le 1$, what in the case at hand is transformed into $\chi_{12}^2 \le \chi_{11}^2$.

It is important to note here that the only nonlinearity contribution controls the scaling of the time τ, while the parameter Λ is completely determined by the lattice itself. Thus the nonlinearity sets the time scale, but not the type of the dynamics (see below), which is defined by the lattice.

The Hamiltonian (47) has two fixed points $F_1 = \{z = 0, \phi = 0\}$ and $F_2 = \{z = 0, \phi = \pi\}$: F_1 is a saddle point for $\Lambda < 1/3$ and a local minimum for $\Lambda > 1/3$, while F_2 is always a local maximum (since $\Lambda < 1$). In Fig. 5a we show the phase portrait corresponding to regime for $\Lambda > \Lambda_c = 1/3$.

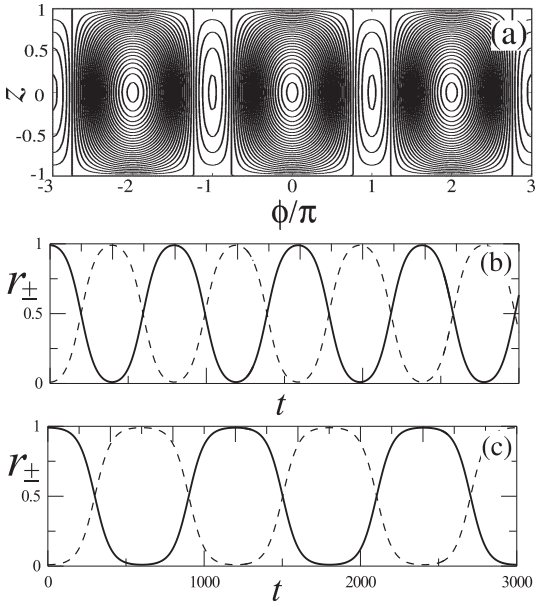

FIG. 5: In (a) phase portrait of the system (45), (46) with $\Lambda = 0.79 > \Lambda_c$ is shown. In (b) and (c) the oscillations of the normalized population imbalance with the initial conditions $z(0) = 0.98$, $\phi(0) = 0$ in (b) and $\phi(0) = \pi$ in (c) correspondingly. Here solid and dashed lines correspond to r_+ and r_-.

In the panels (b) and (c) of Fig.5 we present the dynamics of the "trajectories", $r_\pm(t) = [1 \pm z(t)]/2$, that correspond to the populations r_{2X} and $r_{2X'}$ in the full picture illustrated by Fig. 3. When all particles are initially in the X_2-state one obtains $\{z(0) = 1, \phi(0) = 0\}$, what corresponds to a saddle point. This fact explains why the initial dynamics of the population Fig.3 (b) is constant. By time, however numerical errors accumulate what results in motion of a system along the separatrix which separates two adjacent regions with different dynamics. In the course of evolution the system having reached the next saddle point jumps from one region to the other where the period of oscillations is different. This process continues and it demonstrates itself through the transitions in dynamics of the populations in Fig.3 (b). In order to verify that the transitions occur due to the fact that the system stays close to the separatrix we impose a small shift by taking initially $r_{2X} = 0.99$ and $r_{2X'} = 0.01$, which corresponds to $\{z(0) = 0.98, \phi(0) = 0\}$. As one can see in Fig. 3 (d) the system immediately starts to oscillate with the fixed period. This can be interpreted as the oscillations around the fixed point F_1 [c.f. Fig. 5 (b)]. By comparing the ratio between the periods in different regions near the separatrix, in Fig.5 (b), with the ratio between different times in Fig.3 (b), we found that they are 1.4 and 1.2 respectively.

Returning to Fig. 3, one can observe that the particle transfer due to the intra-band tunneling is accompanied by small oscillations of the density amplitude. After some time the MI is developed. From the first sight this dynamics looks surprising because the energy interchange occurs between two stable states. However, by inspecting the initial state in the points of high symmetry of the first five bands we found that due to inherent inaccuracy of the numerical orthogonalization procedure initial data have nonzero contributions ($\sim 10^{-4} \div 10^{-5}$) from the unstable points of higher bands (for example, in the case of Fig.5 (a), (b) we have also contribution from the unstable points $r_{3X'} \approx 1.3 \times 10^{-5}$ and $r_{5X} \approx 1.2 \times 10^{-5}$). These small contributions of unstable states are consistent with the estimation of the time of MI development.

B. Accelerated deep optical lattice

1. *LZ tunneling starting from a stable state.*

Now we turn to the numerical study of tunneling in an accelerating OL. Along this Section we consider acceleration of a deep OL having the band structure depicted in Fig.1 (d). We start with the case when initially only a state X_1 is populated and the acceleration is applied in the x-direction, $\mathbf{a} = (a_x, 0)$. The results are summarized in Fig.6 (a), (b) where the populations are obtained at instants when the running OL having passed an integer number of period returns to its initial position. In all our simulations we observed that the high symmetrical Γ- and M-states do not become significantly populated during the dynamics.

Considering acceleration applied in the x-direction in

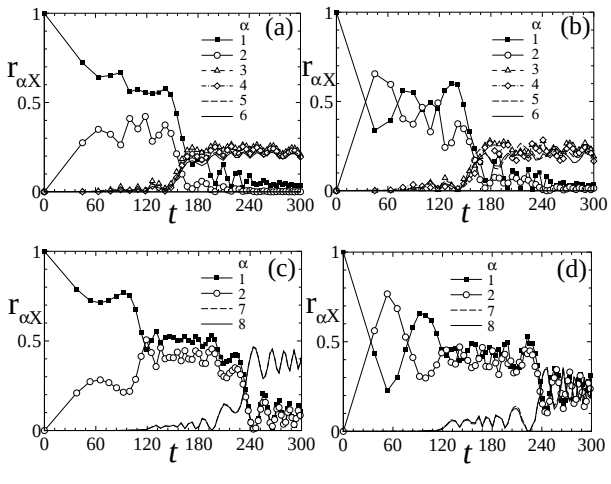

FIG. 6: Dynamics of populations of the lowest bands in X-points with applied acceleration $a_x = 5 \times 10^{-4}$, $a_y = 0$ in [(a),(b)] and with $a_x = a_y = \frac{5}{\sqrt{2}} \times 10^{-4}$ in [(c),(d)]. In [(a),(c)] the linear, $\sigma = 0$, and in [(b),(d)] the nonlinear, $\sigma = 1$, regimes with $N = 20$ are shown. Different symbols stand for populations of X-points (the lines are guides for an eye).

the linear case ($\sigma = 0$) in Eq. (1) [see Fig. 6 (a)], we observe three different regimes. First, during the initial stage the atoms tunnel into the second band implying increase of the population of the X_2-state. This regime, at $t \approx 60$ is changed to balanced distribution of atoms between X_1 and X_2 states, which lasts until $t \approx 150$. This stage of the evolution can be explained due to the large energy difference between the states X_2 and $X_{3,4,5,6}$. In our numerics the evolution is ended up in the particle transfer to the upper states. We inspected the eight lowest bands and found that the process is accompanied by developing rather complex spatial structures of the atomic distribution. Since the states $X_{3,4,5,6}$ have very close energies, their populations reveal almost synchronous behavior, as this is illustrated in Fig. 6 (a).

The nonlinear LZ tunneling has two additional features [see Fig. 6 (b)], compared to the linear one. The initial stage of the tunneling from X_1 to X_2 is ended at earlier times, $t \approx 40$, and during the second stage the dynamics reveals significant Rabi oscillations between the states. Such oscillations occur due to the cross-phase-modulation terms [see the two-state models (20) or (26)] and are characterized by a characteristic period $t_{Rabi} \approx 100$. Taking into account that now the coupling coefficient κ (27) computed between the two X-states $\kappa \approx 0.011$ we find that the analytical estimate for the same time following from the two-state approximation yields $1/\kappa \approx 90$, which is sufficiently good estimate, taking into account that, strictly speaking, the two-state approximation is not valid any more. In the third stage one observes tunneling of the atoms to the upper bands.

In order to understand how tunneling is affected by the direction of acceleration, we show in Fig.6 (c), (d) the results for $a_x = a_y$. We obtained them in such a way that the total modulus of the acceleration is the same as in Fig.6 (a),(b). One can observe the two following changes in the tunneling process. First, exchange between the first and second bands is much stronger: during the second stage of evolution, $120 \lesssim t \lesssim 200$, the second band acquires larger population than the first band. Second, after the instability is developed at $t > 200$ the atoms start to populate 7-th and 8-th bands while $3-6$-th bands remain negligibly populated.

This last phenomenon can be explained by the symmetry of the system. Indeed, let us consider the lowest eight BZs shown in Fig. 1 (b). Departing from the X_1 point one finds the closed high-symmetry points located along the direction $(1,1)$, which coincides with the direction of acceleration, to be the $X_{7,8}$ points, while along the direction $(1,0)$, i.e. along the direction of acceleration shown in Fig. 6 (a),(b), one finds the closed points $X_{3,4,5,6}$.

2. *LZ tunneling starting from an unstable point.*

Let us consider now the situation when initially all particles are placed in the unstable point M_1. In Fig.7 we present linear and nonlinear dynamics of the populations of the lowest bands when the acceleration is applied in (1,0) and in (1,1) directions. In the panels (a) and (b) one observes that the three lowest bands participate in the exchange of particles, which can be explained by the fact that the energy differences between the states M_1, M_2 and M_2, M_3 are of the same order [see Fig. 1 (d)]. Moreover, the population of the third band becomes larger than the population of the two lowest band.

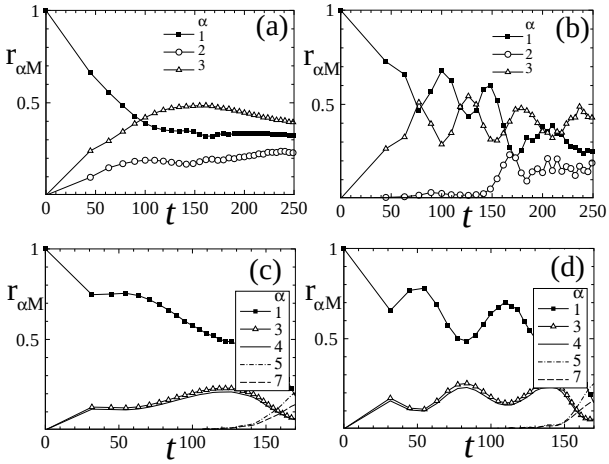

FIG. 7: Dynamics of populations of the lowest bands in the M-point subject to the acceleration $(a_x, a_y) = (5 \times 10^{-4}, 0)$ with $N = 20$ in [(a),(b)] and to $a_x = a_y = 5 \times 10^{-4}$ with $N = 10$ in [(c),(d)]. In [(a),(c)] linear $\sigma = 0$ and in [(b),(d)] nonlinear $\sigma = 1$ regimes are shown.

In the linear case the third stage of the evolution has not been reached for the time $t \lesssim 250$ (this time was

sufficient for transfer to upper bands in all other cases considered so far). Thus the effect of the nonlinearity is much more pronounced, than in the case of tunneling from the stable X-point. Now the nonlinearity gives rise to the Rabi oscillations between the first and the third bands accompanied by strong attenuation of the population of the second band. One can interpret this phenomenon by means of the definition of the nonlinear coefficients $\chi_{\alpha\beta}$ [see (21)], which are responsible for the exchange of atoms between α-th and β-th bands, and from the parity of the BFs bordering a gap: BFs of the bands with different parity have also different parity and, therefore, atomic transition induced by the nonlinearity between first and third bands is more favorable than the oscillations between first and second bands.

The results shown in Fig. 7 (c),(d) indicate that change of the direction of the acceleration results in significant variations in dynamics of populations. Namely, as one can see in Fig.7 (c), where the direction of acceleration coincides with the direction of the symmetry axis (1,1), in the linear case there occurs a monotonic transfer of atoms from the first band to the upper bands, populating almost equally M points in the third and forth bands, with tunneling to the upper bands at later times. Remarkably, the nonlinearity does not affect much the tunneling in this case [c.f. Figs. 7 (b) and 7 (d)], giving rise only to relatively weak oscillations of the populations.

3. LZ tunneling with broken symmetry between X and M states.

Now we focus on the situation when initially two states with different symmetry occupied, namely, X- and M-states. Specifically, in the case of the resonant tunneling presented in Fig.1 (d), we consider the two following configurations: i) almost all particles are in the X_1-state while only small number of particles are in the state M_1 [see Fig. 8] and ii) almost all particles populate the state M_1 while only small number of particles are in the X_1-state [see Fig. 9].

In order to verify whether there exists tunneling between X- and M-states in we calculated the sum of the populations of the eight lowest bands, $\sum_\alpha r_{\mathrm{X,M}}$, in each symmetrical point in the linear and nonlinear regimes. The results are presented in Figs. 8 (e) and 9 (e). The thick dashed and thin dashed lines which represent populations in X- and M-points indicate that particles in X- and M-points conserve their initial population and thus behave independently. It means that in the case of broken symmetry the pure acceleration couples different bands but does not couple different symmetry points. In the presence of the nonlinearity (thick solid and thin solid lines) the evolution of populations reveals Rabi oscillations of populations between X- and M-points which occur due to cross-phase-modulation. We note that this effect without acceleration was observed in [2].

The tunneling from the M- to the X-state, shown in Fig.9 is significantly larger than in the case when particles tunnel from X- to M-state presented in Fig.8 what reveals extremely strong effect of the instability which at very early times results in equal redistribution of atoms between the two high-symmetry points.

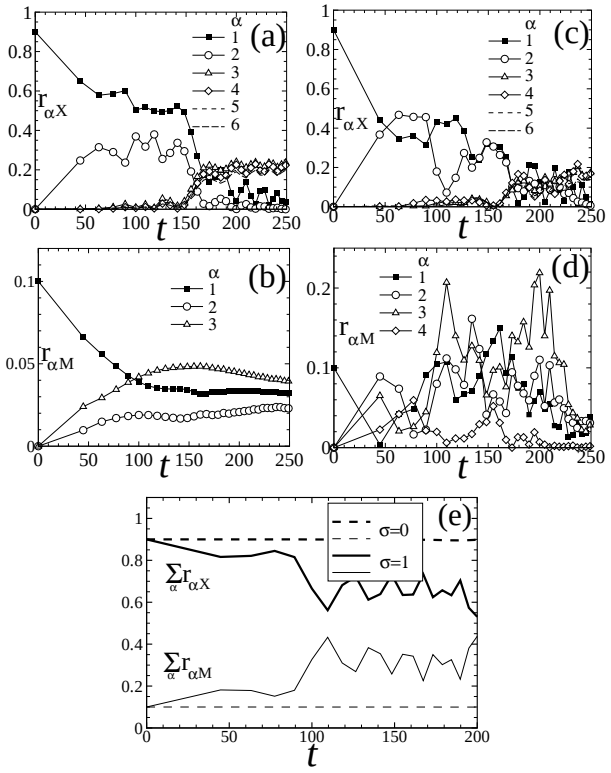

FIG. 8: In (a), (b) linear, $\sigma = 0$, and in (c), (d) nonlinear, $\sigma = 1$, dynamics of the populations of the lowest bands in X- and M-points with acceleration $(a_x, a_y) = (5 \times 10^{-4}, 0)$ with $N = 20$ are presented. In the panels (a) and (c) populations in the X-point and in the panels (b) and (d) populations in the M-point are shown. Initial distribution of the particles is $r_{1X} = 0.9$ and $r_{1M} = 0.1$. Dynamics of the sum of the populations in the X- (thick solid and dashed lines) and in the M-points (thin solid and dashed lines) in the linear (dashed lines) and nonlinear (solid lines) regimes is shown in (e).

C. LZ tunneling in a shallow lattice

Now we turn to the case of the shallow OL corresponding to Fig.1 (f). We start with situation when all particles populate the X_1-point. By accelerating the OL in the linear regime one can see in Fig.10 (a), (b) that small number of particles succeeded to pass to the upper bands and after some time interval (in our case $t \approx 300$) the population of the first five bands becomes stable. The peculiarity of this process stems from the fact that after $t \approx 200$ the population of the third and fourth bands starts to exceed the population of the second band. This effect can be explained by the difference in the effective mass of these bands by taking into account band struc-

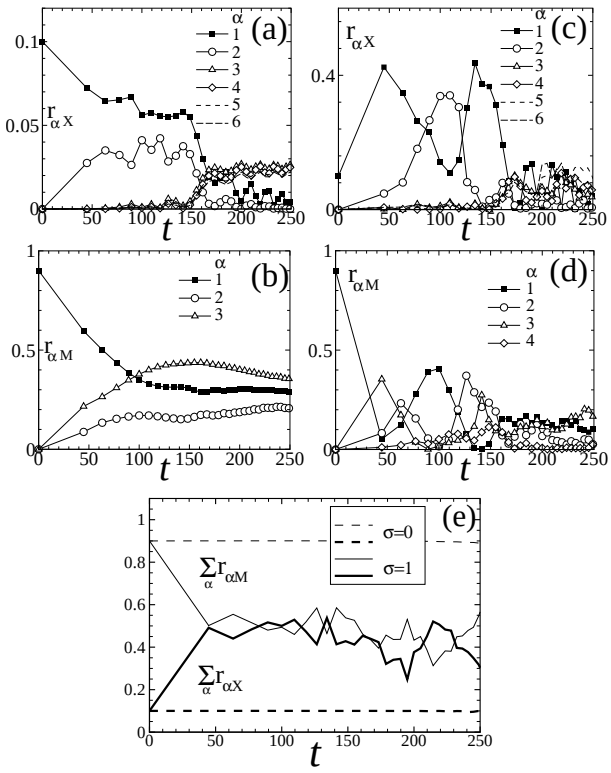

FIG. 9: The same as in Fig.8 with initial distribution of the particles $r_{1M} = 0.9$ and $r_{1X} = 0.1$.

ture from Fig.1 (f) the first, third and fourth bands have the negative effective masses while the second and fifth bands have the positive ones.

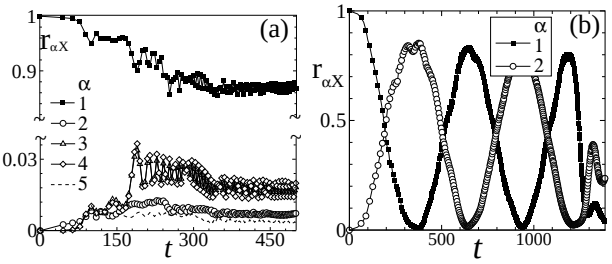

FIG. 10: Dynamics of projections at the X-point with applied acceleration $a_x = 5 \times 10^{-4}$ in (a) the linear case, $\sigma = 0$ and in (b) the same as in (a) with the presence of nonlinearity, $\sigma = 1$. Here $N = 10$. Other parameters are $V_0 = -0.05$ and $\varepsilon = 0.25$ [the band structure is shown in Fig.1 (f)]. Different symbols denote the projections to the α-bands at the X-point calculated at time when the OL returns to the initial position (thin lines are guides for an eye).

One observes completely different dynamics in the nonlinear case with the same initial conditions as in the linear one. In Fig.10 (c) the population of the particles in the presence of nonlinearity starts to oscillate between the first and the second bands and only very small number of particles transfers into the upper bands. After several periods of oscillations this dynamics evolves into the MI.

The dynamics in the shallow lattice case can be interpreted also in terms of the Fourier powers instead of the Bloch band populations. Indeed, as the theory outlined in the Sec. IV predicts for the times smaller than the time of the instability development, the X-point corresponds to the two-fold quasi 1D resonance, hence predicting only two significant peaks in the Fourier space. Namely, if we assume that the initial condition is broad enough in the real space, e.g. a Gaussian possessing width covering many lattice periods, so that the Fourier transform will be a narrow peak, then one can use the LZ model (35) (we notice, that while Gaussian distribution of the density can be substituted by any other one of the same spectral width, it can be created experimentally by first loading the condensate in a parabolic trap at low density, or alternatively sufficiently small wavelength, and subsequently switching on the optical lattice with simultaneous switching off the parabolic trap).

We observe excellent agreement in the linear tunneling regime and a good quantitative correspondence between the LZ models and the full PDE. For instance, in Fig. 11 the numerical results and theory for tunneling at the M-point in the linear case are compared in the case of four-fold resonance. One should keep in mind that for the initial value of the Bloch index we take into account a time shift in the LZ model. In the nonlinear case, however, the theory poorly corresponds to the numerical results, though there is excellent qualitative correspondence easily observed in the Fourier space (for instance, in the number of significant Fourier peaks).

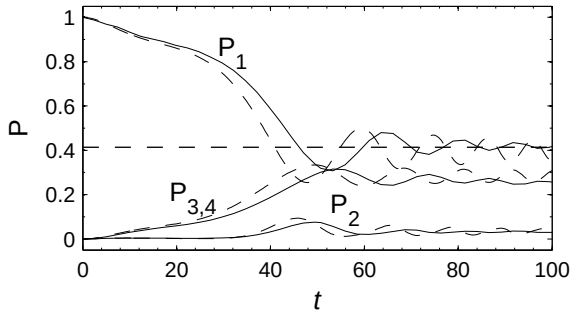

FIG. 11: Comparison of the LZ model with full PDE in the linear case. We use the integrated powers of the Fourier transform of the order parameter Ψ (solid lines) and the squared absolute values of the LZ coefficients (dashed lines). The horizontal line indicates the theoretical prediction according to formula (42). Here $V_0 = 0.025$, $\varepsilon = -1$ and $(a_x, a_y) = (0.01, 0)$. The Gaussian initial condition for Ψ with width of eight lattice periods are used.

VI. CONCLUSION

In the present work we have carried out extensive analytical and numerical analysis of the nonlinear tunnel-

ing of Bose-Einstein condensates in static and accelerating two-dimensional lattices. We focused on nonseparable potentials possessing different band gap structures: having a full gap, no gap, and satisfying the resonant conditions with the full gap vanishing. We investigated different initial atomic distributions in the highly symmetric states, which in the nonlinear case can be either stable or modulationaly unstable, showing substantially different evolutions. We also studied the effect of the direction of the lattice acceleration on the nonlinear tunneling. Within analytical description of the process, we developed several two- and three-mode models, assuming that only a few states are occupied by the atoms.

We found that two-mode models accurately describe the tunneling before instabilities are developed, in the cases when either two respective states are initially populated or tunneling occurs between the two stable states, as this is the case of intra-band tunneling. The early stage evolution is dominated by the Rabi oscillations. Otherwise the two-mode models, although giving useful qualitative hints for understanding of tunneling and even estimates the characteristic times of the process, in general do not describe adequately all the peculiarities of the phenomenon. This deficiency can be explained by the fact that we deal with spatially distributed systems, which in the nonlinear case develop instabilities induced by the two-body interactions, which in their turn result in emergence of spatial coherent structures which are associated with population of higher bands. Moreover, a two-dimensional band structure possesses such peculiarities as states having tensor of the inverse reciprocal masses with components of different signs, what naturally diversifies dynamical scenarios of the tunneling and the symmetry of the developed patterns. We also found that in accelerating lattices the instability phenomenon is much more pronounced and is developed at relatively early stages of evolution. In the latter case we have shown that the direction of the lattice acceleration is a relevant physical parameter significantly modifying atomic patterns emerging as a result of interplay between tunneling and instabilities.

Acknowledgments

VVK is grateful to D. E. Pelinovsky for letting know about the work [17] prior its publication. Authors thank M. Weitz for providing experimental results prior their publication. VVK is pleased to thank the Department of Mathematics of the University of Castilla - La Mancha for warm hospitality. V.A.B. was supported by the FCT grant SFRH/BPD/5632/2001. VVK acknowledges support of Secretaria de Stado de Universidades e Investigación (Spain) under the grant SAB2005-0195. V.S.S. was supported by the research grants from CNPq and CAPES of Brazil. VAB and VVK were supported by the FCT and FEDER under the grant POCI/FIS/56237/2004. Collaborative work was supported by the agreement GRICES/Czech Academy of Sciences and by COST P11 Action.

APPENDIX A: DETAILS OF MULTIPLE-SCALE EXPANSION

1. Some useful relations

In this paper we use the relations as follows

$$\langle\varphi_{\alpha_1\mathbf{q}_1}|\mathbf{r}|\varphi_{\alpha_2\mathbf{q}_2}\rangle = \langle u_{\alpha_1\mathbf{q}_1}|\mathbf{r}|u_{\alpha_2\mathbf{q}_2}\rangle\delta_{\mathbf{q}_1-\mathbf{q}_2,\mathbf{Q}}\,, \tag{A1}$$

$$\langle u_1|\nabla_{\mathbf{q}}|u_2\rangle = -i\langle\varphi_1|\mathbf{r}|\varphi_2\rangle = -4i\frac{\langle\varphi_1|\nabla|\varphi_2\rangle}{E_2-E_1}$$

$$= -4i\frac{\langle u_1|\nabla|u_2\rangle}{E_2-E_1}\,, \tag{A2}$$

$$\langle\varphi_{\alpha_i\mathbf{q}_i}|\nabla^n|\varphi_{\alpha_j\mathbf{q}_j}\rangle = \delta_{\alpha_i\alpha_j}\delta_{\mathbf{q}_i-\mathbf{q}_j,\mathbf{Q}}\langle\varphi_{\alpha_j\mathbf{q}_j}|\nabla^n|\varphi_{\alpha_j\mathbf{q}_j}\rangle, \tag{A3}$$

(A2) being valid for a periodic BFs bordering gap edges.

2. Derivation of Eqs. (20).

The higher order terms in the expansion (13) are searched to be orthogonal to the leading order term ψ_1: $\langle\varphi_{1,2}\mid\psi_j\rangle = 0$ $(j=2,3)$. Therefore we represent ψ_2 as

$$\psi_2 = \sum_{\alpha,\mathbf{q}} B_{\alpha\mathbf{q}}(\mathbf{r}_1,t_1)\varphi_{\alpha\mathbf{q}}e^{-iEt_0}, \tag{A4}$$

and choose the coefficients $B_{\alpha\mathbf{q}}(\mathbf{r}_1,t_1)$ in the form

$$B_{\alpha\mathbf{q}} = B^{(1)}_{\alpha}\delta_{\mathbf{q}-\mathbf{q}_1,\mathbf{Q}}(1-\delta_{\alpha\alpha_1}) + B^{(2)}_{\alpha}\delta_{\mathbf{q}-\mathbf{q}_2,\mathbf{Q}}(1-\delta_{\alpha\alpha_2}), \tag{A5}$$

what justifies the formula (18).

In order to obtain (19) we substitute (A4) with (A5) into (14) what yields

$$\sum_{\alpha\neq\alpha_1}\left[E_\alpha(\mathbf{q}_1)-E\right]B^{(1)}_{\alpha}\varphi_{\alpha\mathbf{q}_1} + \sum_{\alpha\neq\alpha_2}\left[E_\alpha(\mathbf{q}_2)-E\right]B^{(2)}_{\alpha}\varphi_{\alpha\mathbf{q}_2}$$
$$= i\partial_{t_1}A_1\varphi_1 + i\partial_{t_1}A_2\varphi_2 + 4\nabla_1A_1\cdot\nabla_0\varphi_1 + 4\nabla_1A_2\cdot\nabla_0\varphi_2. \tag{A6}$$

By applying $\langle\varphi_{1,2}\mid$ to the both sides of this equation and using (A3) we obtain

$$\partial_{t_1}A_j - \mathbf{v}\nabla_1A_j = 0 \quad \text{for} \quad j=1,2. \tag{A7}$$

Next we apply $\langle\varphi_{\alpha_j,\mathbf{q}_{1,2}}|$ into (A6) and use (A3) and (19). This yields for $j=1,2$ and $\alpha\neq\alpha_j$

$$B_\alpha^{(j)}=4\frac{\langle u_{\alpha\mathbf{q}_j}\mid\nabla_0\mid\varphi_j\rangle}{E_\alpha(\mathbf{q}_j)-E}\nabla_1 A_j. \tag{A8}$$

The equations of the third order (20) are obtained from (9) by using the orthogonality conditions $\langle\varphi_{1,2}\mid\mathcal{F}_3\rangle=0$, the explicit form of ψ_2 given by (18) and (A8), and the definition (12).

3. Derivation of Eqs. (26).

Now the coefficients $B^{(j)}_{\alpha\mathbf{q}}(\mathbf{r}_1,t_1)$ are as follows

$$B^{(j)}_{\alpha\mathbf{q}}=\delta_{\mathbf{q}-\mathbf{q}_j,\mathbf{Q}}(1-\delta_{\alpha\alpha_j})B^{(j)}_\alpha,\quad j=1,2 \tag{A9}$$

what justifies the formula (25).

In order to obtain (19) we substitute (25) with (A9) into (14), separate terms corresponding to the main harmonics [$\propto\exp(-iE_{1,2}t_0)$] what yields ($j=1,2$)

$$\sum_{\alpha\neq\alpha_j}\left[E_j-E_\alpha(\mathbf{q}_j)\right]B^{(j)}_\alpha\varphi_{\alpha\mathbf{q}_j}=-i\partial_{t_1}A_j\varphi_j -4\nabla_1 A_j\cdot\nabla_0\varphi_j. \tag{A10}$$

By applying $\langle\varphi_{1,2}|$ to the both sides of this equation and using (11) we compute Eqs. (A7). Next we apply $\langle\varphi_{\alpha_j,\mathbf{q}_{1,2}}|$ to (A10) and use (A3) and (19) . This yields for $j=1,2$ and $\alpha\neq\alpha_j$

$$B_\alpha^{(j)}=4\frac{\langle u_{\alpha\mathbf{q}_j}\mid\nabla_0\mid\varphi_j\rangle}{E_\alpha(\mathbf{q}_j)-E_j}\nabla_1 A_j\,. \tag{A11}$$

The equations (26) are obtained from (9) after separating the two main harmonics, using the orthogonality conditions $\langle\varphi_{1,2}\mid\mathcal{F}_3\rangle=0$, a particular explicit form of ψ_2, (A11), and the definition (12).

[1] V. V. Konotop, P.G. Kevrekidis, and M. Salerno, Phys. Rev. **A** 72, 023611 (2005).

[2] V. A. Brazhnyi, V. V. Konotop, and V. Kuzmiak, Phys. Rev. Lett. **96**, 150402 (2006).

[3] O. Morsch, J. H. Muller, M. Cristiani, D. Ciampini, and E. Arimondo, Phys. Rev. Lett. **87**, 140402 (2001); M. Cristiani, O. Morsch, J. H. Muller, D. Ciampini, and E. Arimondo Phys. Rev. A **65**, 063612 (2002); C. Sias, A. Zenesini, H. Lignier, S. Wimberger, D. Ciampini, O. Morsch, and E. Arimondo, Phys. Rev. Lett. **98**, 120403 (2007).

[4] M. Jona-Lasinio, O. Morsch, M. Cristiani, E. Arimondo and C. Menotti, cond-mat/0501572.

[5] S. Wimberger, R. Mannella, O. Morsch, E. Arimondo, A. R. Kolovsky, and A. Buchleitner, Phys. Rev. A **72**, 063610 (2005).

[6] C. Sias, A. Zenesini, H. Lignier, S. Wimberger, D. Ciampini, O. Morsch, and E. Arimondo, Phys. Rev. Lett. **98**, 120403 (2007).

[7] G. Ritt, C. Geckeler, T. Salger, G. Cennini, and M. Weitz, Phys. Rev. A **74**, 063622 (2006); T. Salger, G. Ritt, C. Geckeler, S. Kling, and M. Weitz, (in preparation).

[8] B. Wu and Q. Niu, Phys. Rev. A **61**, 023402 (2000); O. Zobay and B. M. Garraway, Phys. Rev. A **61**, 033603 (2000).

[9] V. S. Shchesnovich and S. B. Cavalcanti, J. Phys. B: At. Mol. Opt. Phys. **39**, 1997(2006).

[10] V.S. Shchesnovich, S. B. Cavalcanti, J. M. Hickmann, and Yu. S. Kivshar, Phys. Rev. E **74**, 056602 (2006); A. S. Desyatnikov, Yu. S. Kivshar, V. S. Shchesnovich, S. B. Cavalcanti, and J. M. Hickmann, Optics Lett. **32**, 325 (2007).

[11] A.R. Kolovsky and H.J. Korsch, Phys. Rev. A **67**, 063601 (2003); D. Witthaut, F.Keck, H.J. Korsch, S. Mossmann, New J. Phys. **6**, 41 (2004).

[12] M. Greiner, I. Bloch, O. Mandel, T. W. Hänsch, and T. Esslinger, Phys. Rev. Lett. **87**, 160405 (2001); M. Greiner, O. Mandel, T. W. Hänsch and I. Bloch, Nature **419**, 51 (2002); H. Moritz, T. Stöferle, M. Köhl, and T. Esslinger, Phys. Rev. Lett. **91**, 250402(2003).

[13] J. M. Ziman *The principles of the Theory of Solids* (Cambridge: Cambridge University Press, 1972).

[14] P. Schlagheck and S. Wimberger, Appl. Phys. B **86**, 385 (2007).

[15] B. B. Baizakov, V. V. Konotop, and M. Salerno, J. Phys. B: At. Mol. Opt. **35**, 5105 (2002).

[16] A. Newell and J. Moloney, *Nonlinear Optics* (Addison-Wesley, Redwood City, CA, 1992).

[17] T. Dohnal, D. Pelinovsky, and G. Schneider, "Coupled-mode equations and gap solitons in a two-dimensional nonlinear elliptic problem with a separable periodic potential" (to be submitted).

[18] W. V. Houston, Phys. Rev. **57**, 184 (1940).

[19] L. D. Landau, Phys. Z. Sowjetunion **2**, 46 (1932); C. Zener, Proc. R. Soc. London A **137**, 696 (1932); E. Majorana, Nuovo Cimento **9**, 43 (1932).

[20] S. Brundobler and V. Elser, J. Phys. A: Math. Gen. **26**, 1211 (1993); A.V. Shytov, Phys. Rev. A **70**, 052708 (2004).